Full waveform inversion of reflection seismic data for ocean temperature profiles

Warren T. Wood,[1] W. Steven Holbrook,[2] Mrinal K. Sen,[3] and Paul L. Stoffa[3]

Received 15 October 2007; revised 10 January 2008; accepted 24 January 2008; published 23 February 2008.

[1] We show that ocean temperature profiles can be accurately recovered using only acoustic methods employed at the sea surface. Using a towed air gun array and a hydrophone streamer, thermohaline boundaries are ensonified at a suite of frequencies and angles, yielding travel time trajectories and reflectivities. These data are inverted via full waveform inversion to estimate sound speed and, subsequently, a temperature profile. The high lateral data density of the seismic technique offers the potential of acoustically derived temperature profiles to be used to constrain models of ocean mixing and internal waves. Results on realistic synthetic data show that sound speed can be recovered with arbitrary accuracy when using broadband data, with known source function and recording geometry. Application to field seismic data (corroborated by expendable bathythermograph) shows that even with a seismic acquisition system not specifically calibrated for seismic oceanography, temperature contrasts within the ocean can be recovered to within one degree Celsius.
Citation: Wood, W. T., W. S. Holbrook, M. K. Sen, and P. L. Stoffa (2008), Full waveform inversion of reflection seismic data for ocean temperature profiles, *Geophys. Res. Lett.*, *35*, L04608, doi:10.1029/2007GL032359.

1. Background and Motivation

[2] Marine reflection seismology has recently been shown capable of producing detailed images of oceanic thermohaline finestructure at lateral resolution of ~10 m [*Holbrook et al.*, 2003]. Images of finestructure have been produced in numerous ocean settings, including fronts [*Holbrook et al.*, 2003; *Noguchi et al.*, 2006; *Tsuji et al.*, 2005; *White et al.*, 2006], Meddies [*Klaeschen et al.*, 2006; *Pinheiro et al.*, 2006], intrathermocline lenses [*Bullock*, 2006], warm-core rings [*Seymour et al.*, 2006], water-mass boundaries [*Huthnance et al.*, 2006; *Nandi et al.*, 2004], and thermohaline staircases [*Nandi et al.*, 2006]. While the images alone have intrinsic interest, a key topic of current research in "seismic oceanography" is the extraction from seismic data of quantitative information on physical oceanographic processes and properties, such as internal-wave spectra [*Holbrook and Fer*, 2005; *Krahmann et al.*, 2006] and temperature contrasts [*Páramo and Holbrook*, 2005]. In this paper we explore the possibility of inverting seismic reflection data for temperature-depth profiles in the ocean, using one-dimensional (1D) full-waveform inversion, demonstrated on seismic data co-located with XBT profiles in the Norwegian Sea.

[3] Seismic oceanography data are especially well suited to one-dimensional waveform inversion approaches, because thermohaline boundaries in the ocean are very nearly flat and horizontal, lateral variations in sound speed are small, no converted shear waves are present, and interbed multiples are negligible due to the small reflection coefficients (~0.001). Through full waveform inversion [e.g., *Singh et al.*, 1993; *Wood et al.*, 1994; *Korenaga et al.*, 1997], every reflection within the water column is modeled simultaneously, resulting in a 1-D profile of sound speed, which can then be readily converted to temperature via an equation of state [e.g., *Chen and Millero*, 1977]. Although the inversion algorithm is capable of distinguishing independently varying density and sound speed, density contrasts are typically much smaller than sound speed contrasts in the ocean and contribute little to the reflectance in the Norwegian Sea data set used here [*Páramo and Holbrook*, 2005], so we assume for this study that all reflectivity in the water column is associated with sound speed contrasts.

2. Inversion Method

[4] The groundwork for the class of problems and solutions used here has been discussed extensively by *Menke* [1989] and *Tarantola* [1987], and the application to reflection seismic data is based on the work of *McAulay* [1985, 1986], *Dietrich and Kormendi* [1990], *Amundsen and Ursin* [1991], and *Wood et al.* [1994]. We define the general forward problem as

$$\mathbf{d} = \mathbf{g}(\mathbf{m}) + \mathbf{v} \tag{1}$$

where $\mathbf{m}$ is a vector of n_{mod} model parameters (in this case sound speeds), $\mathbf{g}$ is a non-linear operator, in this case containing information on acoustic wave propagation and the experimental configuration, $\mathbf{v}$ is a vector of additive noise, and $\mathbf{d}$ is a vector of n_{dat} data (in this case waveform amplitudes) that would be observed if the water column sound speed was perfectly described by $\mathbf{m}$, if $\mathbf{g}$ was a perfect theoretical relation, and if $\mathbf{v}$ was identically zero. (Vectors and vector functions of vectors are cast in lower case bold type while matrices are cast in uppercase bold type). The inverse problem can then be defined as

$$\mathbf{m} = \mathbf{y}(\mathbf{d} - \mathbf{v}), \tag{2}$$

[1]Naval Research Laboratory, Stennis Space Center, Mississippi, USA.
[2]Department of Geology and Geophysics, University of Wyoming, Laramie, Wyoming, USA.
[3]Institute for Geophysics, University of Texas at Austin, Austin, Texas, USA.

0094-8276/08/2007GL032359

where **v** can be absorbed into the data vector, and **y** is a generalized inverse, the structure of which is the subject of much discussion in the literature, (e.g., monographs by *Tarantola* [1987] and *Menke* [1989]). For linear problems and wisely chosen objective functions a single evaluation of the slope and curvature of the objective function at any point can be used to generate the best possible estimate of the location of the objective function minimum and optimal model. If the problem is almost linear, then an evaluation of the slope and curvature result in an improved, but not optimal model estimate, and may have to be re-evaluated, making the solution iterative, but still linearizable (as is the case for sound speed in this study). We use the least squares objective function, S, defined in vector notation as;

$$2S[\Delta\mathbf{d}^t\mathbf{C}_D^{-1}\Delta\mathbf{d} + \Delta\mathbf{m}^t\mathbf{C}_m^{-1}\Delta\mathbf{m}],$$

with

$$\Delta\mathbf{d} = [\mathbf{d}_{syn} - \mathbf{d}_{obs}] = [\mathbf{g}(\mathbf{m})_n - \mathbf{d}_{obs}],$$

and

$$\Delta\mathbf{m} = [\mathbf{m}_n - \mathbf{m}_o], \tag{3}$$

where $\mathbf{C}_\mathrm{D}$ and $\mathbf{C}_\mathrm{m}$ are prior data and model covariance matrices respectively, and $\mathbf{m}_\mathrm{o}$ and $\mathbf{m}_\mathrm{n}$ are model vectors containing the a priori and n^{th} trial model parameters, respectively, (superscript t denotes transpose). The vector $\mathbf{d}_\mathrm{obs}$ contains the observed data, and $\mathbf{d}_\mathrm{syn}$ contains the synthetic data generated from the n^{th} model iteration by the operator **g**. The vector $\mathbf{d}_\mathrm{syn}$ can also be expressed as the vector function, $\mathbf{g}(\mathbf{m}_\mathrm{n})$. The objective function consists of both a model and data error, and it is the combination of these errors that is to be minimized. Even if the data are matched exactly the objective function may be quite large if the corresponding model is far from the prior model. Errors in the theory of the forward modeling $\mathbf{g}(\mathbf{m}_\mathrm{n})$ take the same form as, and are absorbed into, the data covariances in $\mathbf{C}_\mathrm{D}$. For this study these modeling errors occur when the ocean structure is not 1-D (dipping or discontinuous layers), not isotropic (wave speeds are directionally dependent), or inelastic (wave amplitudes are attenuated as a function of time).

[5] For this study we chose the least squares error solution defined above with Newton's method of minimization. The convergence for linear problems is quick, the mathematical foundation for the solution is well known [*Tarantola*, 1987; *Menke*, 1989], and a quantitative estimate of the variance (uncertainty) in the solution can be easily obtained from the curvature of the error surface at the point of minimum error.

[6] The iterative form of Newton's method can be written in multi-dimensional form [*Tarantola*, 1987] as

$$\mathbf{m}_{n+1} = \mathbf{m}_n - [\partial^2\mathbf{S}/\partial\mathbf{m}^2]_n^{-1}[\partial\mathbf{S}/\partial\mathbf{m}]_n \tag{4}$$

where ∂ denotes the partial derivative, and **S** is the value of the objective function. Here both the slope and curvature of the model space at the nth iteration are used to find the next, or n + 1th model estimate.

[7] Taking the derivative of S to find the local multidimensional slope yields

$$[\partial S/\partial m]_n = \mathbf{G}_n^t\mathbf{C}_D^{-1}\Delta\mathbf{d} + \mathbf{C}_m^{-1}\Delta\mathbf{m} \tag{5}$$

where the matrix $\mathbf{G}_\mathrm{n}$ (sensitivity or Frechet derivative matrix) contains the sensitivity of each data parameter to each model parameter

$$G_n^{ij} = [\partial d^i/\partial m^j]_n \tag{6}$$

[8] Taking the second derivative to find the local multidimensional curvature yields;

$$[\partial^2\mathbf{S}/\partial\mathbf{m}^2]_n \approx \mathbf{G}_n^t\mathbf{C}_D^{-1}\mathbf{G}_n + \mathbf{C}_m^{-1}, \tag{7}$$

where the neglected term is small when the forward problem is nearly linear.

[9] Combining equations (4), (5), and (7) gives the expression used in this study,

$$\mathbf{m}_{n+1} = \mathbf{m}_n + [\mathbf{G}_n^t\mathbf{C}_D^{-1}\mathbf{G}_n + \mathbf{C}_m^{-1}]^{-1}[\mathbf{G}_n^t\mathbf{C}_D^{-1}\Delta\mathbf{d} + \mathbf{C}_m^{-1}\Delta\mathbf{m}], \tag{8}$$

where $\mathbf{G}_\mathrm{n}$ is re-computed at each iteration, and each of the other components on the right hand side is known at the start of the inversion. The $\mathrm{n_{mod}}$ x $\mathrm{n_{mod}}$ matrix, $[\mathbf{G}_\mathrm{n}^\mathrm{t}\,\mathbf{C}_\mathrm{D}^{-1}\,\mathbf{G}_\mathrm{n} + \mathbf{C}_\mathrm{m}^{-1}]$, referred to as the Hessian, is solved via singular value decomposition (SVD) [e.g., *Menke*, 1989].

3. Application to Synthetic Seismic Data

[10] To apply equation (8) to seismic reflection data, we parameterize the problem such that the model is a series of sound speeds corresponding to layers in the water column whose time thicknesses are held constant at the seismic data sample increment of 0.004 seconds. This ensures that any layer that can affect the seismic data can be completely modeled, i.e. any synthetic seismogram can be reproduced exactly. We parameterize the data as frequency domain, plane-wave seismograms as obtained by a Fourier-Hankel transform of a common midpoint (CMP) gather. This allows for use of the very efficient reflectivity method [*Kennett and Kerry*, 1979] as the forward operator $\mathbf{g}(\mathbf{m})$ in equation (1). Our use of the reflectivity method also requires knowledge of the source function (wavelet), whose shape (phase) was determined by iteratively modeling frequency component phases to minimize the total energy of a series of field data traces [*Wood*, 1999].

[11] The degree to which each of the data and model misfits are minimized is controlled by the a priori covariances in $\mathbf{C}_\mathrm{m}$ and $\mathbf{C}_\mathrm{D}$. For the trials presented in this study both $\mathbf{C}_\mathrm{m}$ and $\mathbf{C}_\mathrm{D}$ are assumed to be purely diagonal matrices, with each diagonal a constant value. The data and model covariances, which correspond to the squared uncertainties, were chosen as 0.01 and 300 respectively. Note that these parameters can also be regarded as regularization parameters that introduce stability in the inversion. The chosen values result in the data misfit being much more heavily weighted than the model misfit, appropriate in this case where we are much less certain about the a priori model than about the observed data.

[12] To test the sensitivity of the inversion we generate a synthetic seismogram based on the same Norwegian Sea seismic data and coincident XBT (expendable bathythermograph) profiles presented by *Páramo and Holbrook* [2005], displayed here in the intercept time-slowness (Tau-p) domain, rather than the frequency-slowness (ω-p) domain for ease of interpretation (Figure 1b). The temperatures from the XBT were converted to sound speed assuming a constant salinity of 32 PSU, and using these sound speeds were converted to time and re-sampled at 4 millisecond intervals (Figure 1a). Errors in overall salinity manifest only at the lowest frequencies (less than 1 Hz), and because an a priori starting model supplies this frequency band, the sensitivity of the inversion to overall salinity is small. The XBT and the wavelet estimated from the data were used to generate the synthetic seismogram shown in Figure 1b.

[13] Two inversion results of ideal synthetic data are presented in Figures 1a–1c, using starting models (red curves) that are 0.0 and 5.0 Hz low pass (cosine tapered from 0 to 5 Hz) versions of the true model, and both performed over the entire 0-125 Hz frequency band of the seismic data. When using the 5 Hz starting model, the algorithm converged to the true model (black curve, Figure 1a), matching the data to within one part in a thousand, leaving only a low amplitude, low frequency residual (Figure 1c). Using the 0 Hz, constant sound speed of 1499 m/s as the starting model, the algorithm accurately recovered the higher frequency portions of the model, but recovery of the lower frequency components is incomplete below the strongest reflection event at about 0.6 seconds (Figure 1a). The degradation is due mainly to the lack of strong reflections in this portion of the data set, whose trajectories drive the recovery of the low frequency model components, hence the low frequency residual in Figure 1c. The higher frequency components of the profile (detail) actually enable the recovery of the lower frequency components (background) through the generation of reflection events.

[14] For the "noiseless" synthetic examples in Figures 1a–1c, the accuracy of the inversion is limited only in that the ratio of the smallest to the largest eigenvalue in the Hessian matrix must be larger than the machine precision. This places the effective noise floor at the level of machine precision, i.e. 10^{-8}, for all synthetic trials in this study, allowing exceptionally low amplitude frequency components to contribute to recovering the thermal profile. Recently reported techniques may eliminate the need to compute the matrix inverse, allowing even greater accuracy [*Sen and Roy*, 2003; *Roy et al.*, 2005].

[15] The successful recovery of the correct temperature-depth profile by the seismic waveform inversion is not merely confirmation that the inversion technique and algorithm work, but rather a demonstration that, for seismic data with typical frequency range of 10-125 Hz, realistic finestructure can be fully resolved to the extent that certain practical conditions, which we discuss next, are met.

4. Application to Field Data

[16] We next apply the inversion to field data coincident with an XBT so the inversion technique can be independently corroborated. The data were originally sampled at 0.002 milliseconds, however, most of the source band was below 125 Hz, so we low pass filtered and re-sampled the data to 0.004 milliseconds. This reduces the number of model parameters, n_{mod}, by a factor of two, greatly facilitating the SVD of the Hessian matrix.

[17] Application of the inversion to field data also requires transforming the data into the plane wave (ω-p) domain [e.g., *Brysk and McCowan*, 1986a, 1986b] and using tapering to minimize the transform artifacts. The inversion is performed over the slowness range p = 0–0.6 s/km, or approximately 0–64 degrees incidence angle. The small group size in the array affects the directivity only slightly (1.5% at 90 Hz and 65 degrees incident angle) so we assume it is negligible.

[18] Both the absolute value, and the angle dependence of the reflection coefficient are required for the inversion. To convert seismic signals to reflection coefficients we compare the water bottom primary and first sea surface multiple [*Warner*, 1990] resulting in a scale factor of 5.0×10^4 +/– 2.0×10^4. The large uncertainty was due to significant interference between the multiple and primary reflections from subsurface stratigraphy. The data scaling error manifests primarily as a constant multiplicative factor to the entire *a posteriori* model, but because the lowest frequencies in the a posteriori model rely almost completely on the lowest frequencies in the a priori model, the inversion at these frequencies is mostly insensitive to scaling error. Within the data band, the scaling errors manifest as an error in the deviation from the smooth background, which can be incorporated into the model uncertainties associated with the smooth starting model. Although not done so here, the scale factor could potentially be included as a model parameter for which to invert.

[19] The observed data in the plane wave domain are shown in Figure 1e, along with the best (smallest) residual from the inversion (Figure 1f), and the model responsible for the best residual (Figure 1d). As in the synthetic data example, two inversion results are presented; corresponding to starting models that are low-pass filtered (cosine taper from 0-30 Hz) versions of the XBT profile. The zero Hz case is extreme and used here for illustrative purposes. In most cases, analyzing the trajectory of the sea bottom reflection can yield an average velocity profile in the 0-1.0 Hz range. The 30 Hz starting model supplies the components that are poorly constrained or missing in the data band (about 25-80 Hz) and the inversion supplies the rest, resulting in a low data residual (Figure 1f). This result also provides a gross check on the inversion, confirming that the algorithm will converge on what we expect is the true model, (i.e. the XBT profile lies very near the position of the global minimum).

[20] Even when a constant sound speed is used as the starting model, the lowest frequency components of the model are well recovered down to the major reflection at 0.6 seconds. There are two exceptions: 1) the shallow portion corresponding to the warm surface waters where the corresponding data were muted due to interference with the direct wave, and 2) the event at about 0.75 s that results from a more gradual thermal transition than the event at 0.6 s, placing it near the low end of the spectrum where recovery is weak. The inset in Figure 1e shows that the magnitude of the temperature step at 0.6 s is recovered

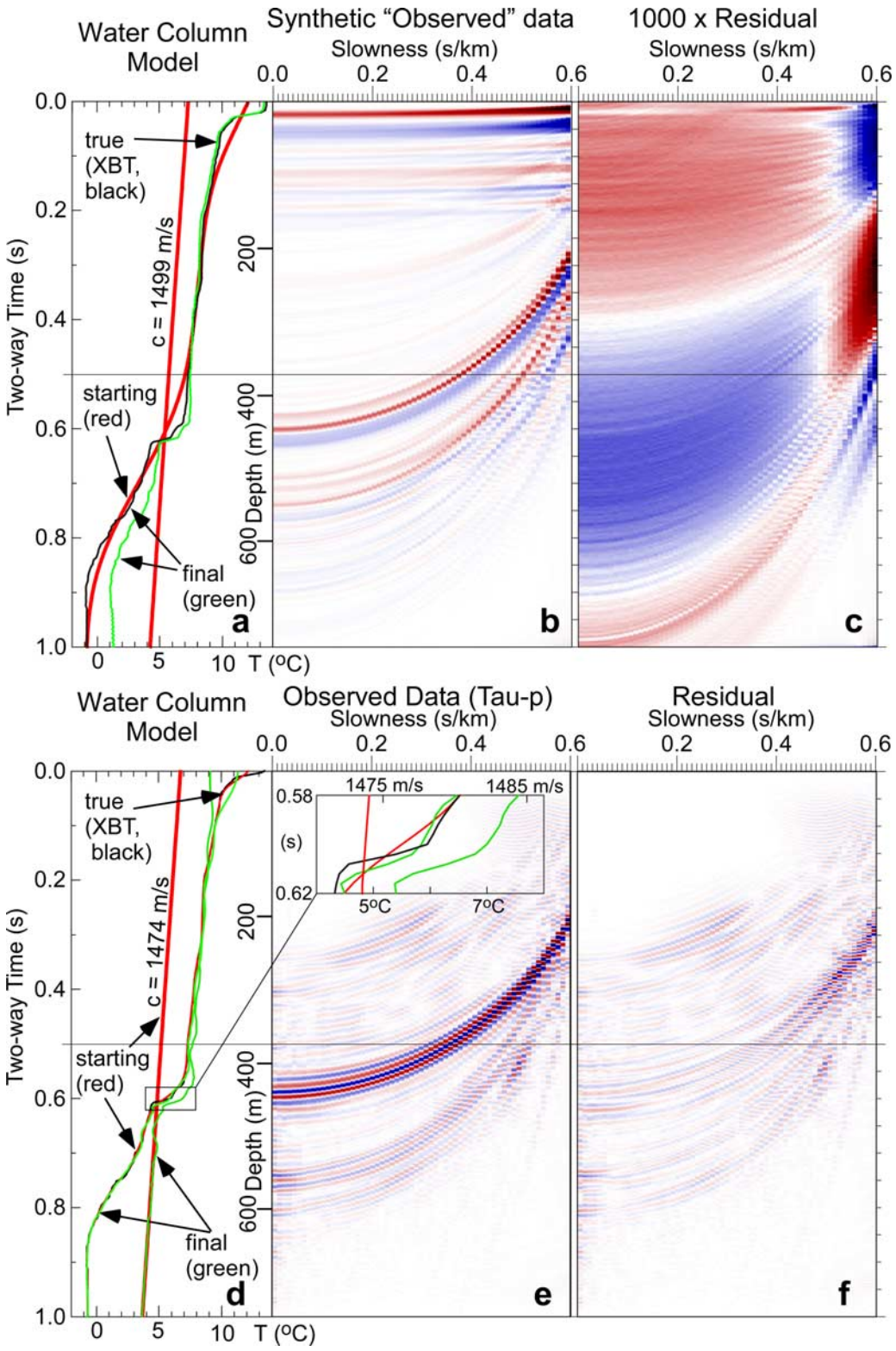

Figure 1. The sound speed profile from (a) an XBT cast (true model, black curve) was used to generate (b) a synthetic data set, used as the observed data in a test of the inversion. The starting models (red curves) are 0 Hz and 5 Hz low pass filtered versions of the true model. The green curve is the inversion from the 0 Hz starting model, and the inversion result from the 5 Hz starting model (not shown) is effectively coincident with the true model, resulting in (c) a data residual (difference between observed and synthetic, magnified one thousand times) that is extremely small. (e) The field data were acquired coincidently with (d) the XBT (black curve), which can be used to independently corroborate the inversion result. The starting models (see Figure 1d, red curves) are 0 Hz and 30 Hz low pass filtered versions of the XBT profile. The two inversion results are shown in green. When the low frequency portion of the model is supplied in the starting model, the inversion result matches the XBT and the (f) data residual is minimized.

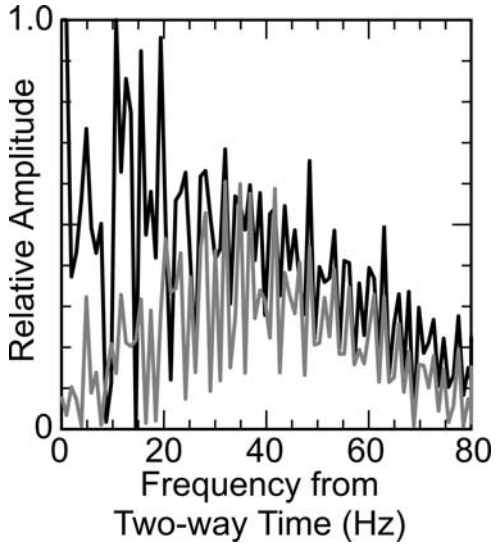

Figure 2. The discrepancy between the spectra of the XBT and inverted sound speed profile using the 0 Hz (black) and 30 Hz (gray) starting model shows that either starting model will result in roughly equal recovery of frequencies above about 30-40 Hz. Supplying frequencies below 30 Hz in the sound speed model (gray) significantly reduces the discrepancy.

accurately regardless of the starting model, but recovery of the absolute temperature requires accurate background (low frequency) components. Figure 2 shows more quantitatively how spectra of the inverted sound speed profiles differ from the spectrum of the XBT. For the profile recovered using the 30 Hz starting model, the spectral difference (gray curve) is much smaller at the lower frequencies, because these frequencies have been supplied by the starting model. The discrepancy is much larger (black curve) for the profile recovered using the zero Hz starting model. Frequency components well within the data band (25-80 Hz) are recovered roughly equally well regardless of the starting model.

[21] Based on the successful recovery of the low frequency components above 0.6 seconds, and the results of the trials on synthetic data, we would expect that had the seafloor reflection been included in the inversion, the seismic data alone would have had the low frequency components necessary to recover the absolute temperature. These components would not need to have been contributed via the starting model. The seafloor reflection was not included in the inversion because the vast difference in amplitude (about 3 orders of magnitude) between seafloor and water column reflections caused significant artifacts in the frequency domain processes (filtering, plane-wave transform, and inversion) used here.

[22] Unlike the synthetic data example, there are small discrepancies between the best-recovered model and the "true" XBT profile. The XBT may not be located at exactly the same position as the CMP. Also, the CMP is composed of several subsequent source firings, acquired up to several minutes and tens of meters apart, over which some averaging is inevitable. Further, each source fire may be different due to irregularities in firing time, air pressure, sea state, or other mechanical phenomena. The irregularities are usually negligible, but may, along with any artifacts of the finite integral transform, manifest either as errors in the wavelet, which can result in unwanted deviations in the final model, or as artifacts in the data that cannot be modeled but may draw the algorithm away from its desired course of convergence. Acquisition irregularities or source wavelet errors are the most likely cause of the approximately 10 Hz undulations in the recovered profiles in Figure 1d, and could likely be significantly mitigated in an experiment designed specifically for seismic oceanography.

5. Conclusions

[23] We have demonstrated that full waveform inversion can recover ocean temperature profiles from surface towed seismic measurements alone. Inversions of synthetic seismic data show the technique can resolve oceanic finestructure at the 5 m vertical scale with arbitrary accuracy. In a test on field data, the accuracy of the recovered profile depends on how well the frequency bands of the seismic data and starting model cover the band of the desired profile, and on the presence of reflections throughout the profile to provide the low frequency components of the profile. The latter requirement can be relaxed if sufficient XBT data are present regionally to provide background temperature-depth profiles for starting models. The recovery of sharp thermal changes is generally more accurate than the recovery of the absolute temperature. With customary seismic equipment and recording techniques, we have estimated the magnitude of a temperature contrast to within approximately 20%, or 0.5 degrees C of its value as measured directly with an XBT. This accuracy could be improved significantly with more accurate measurements of the source wavelet, and broader band data. Our results suggest that augmenting sparse direct temperature measurements (e.g., XBTs) with inversions of seismic data, may result in an effective means of achieving high lateral and vertical resolution thermal cross-sections over extensive regions of the ocean.

[24] **Acknowledgments.** The authors thank the reviewers for their helpful comments. This work was funded by NSF-OCE 0452744 and NSF-OCE 0648620.

References

Amundsen, L., and B. Ursin (1991), Frequency-wavenumber inversion of acoustic data, *Geophysics*, *56*, 1027–1039.

Brysk, H., and D. W. McCowan (1986), A slant stack procedure for point-source data, *Geophysics*, *51*, 1370–1386.

Brysk, H., and D. W. McCowan (1986), Edge effects in cylindrical slant stacks, *Geophys. J. R. Astron. Soc.*, *87*, 801–813.

Bullock, A. D. (2006), Enhanced finestructure around an intrathermocline lens in the Norwegian Sea, *Eos Trans. AGU*, *87*(36), Ocean Sci. Meet. Suppl., Abstract OS13I-04.

Chen, C. T., and F. J. Millero (1977), Speed of sound in seawater at high pressures, *J. Acoust. Soc. Am.*, *62*, 1129–1135.

Dietrich, M., and F. Kormendi (1990), Perturbation of the plane-wave reflectivity of a depth-dependent elastic medium by weak inhomogeneities, *Geophys. J. Int.*, *100*, 203–214.

Holbrook, W. S., and I. Fer (2005), Ocean internal wave spectra inferred from seismic reflection transects, *Geophys. Res. Lett.*, *32*, L15604, doi:10.1029/2005GL023733.

Holbrook, W. S., et al. (2003), Thermohaline fine structure in an oceanographic front from seismic reflection profiling, *Science*, *301*, 821–824.

Huthnance, J., et al. (2006), Imaging the time dependence of water boundaries in the Faroe-Shetland Channel, *Eos Trans. AGU*, *87*(36), Ocean Sci. Meet. Suppl., Abstract OS13I-06.

Kennet, B. L. N., and N. J. Kerry (1979), Seismic waves in a stratified half-space, *Geophys. J. R. Astron. Soc.*, *57*, 557–583.

Klaeschen, D., et al. (2006), Seismic images and properties of a Meddy, *Eos Trans. AGU*, *87*(36), Ocean Sci. Meet. Suppl., Abstract OS13I-03.

Korenaga, J., W. S. Holbrook, S. C. Singh, and T. A. Minshull (1997), Natural gas hydrates on the southeast U.S. margin: Constraints from full waveform and travel time inversions of wide-angle seismic data, *J. Geophys. Res.*, *102*, 15,345–15,365.

Krahmann, G., et al. (2006), Internal wave energy estimated from seismic reflection data, *Eos Trans. AGU*, *87*(36), Ocean Sci. Meet. Suppl., Abstract OS16I-03.

McAulay, A. D. (1985), Pre-stack inversion with plane-layer point source modeling, *Geophysics*, *50*, 77–89.

McAulay, A. D. (1986), Plane layer prestack inversion in the presence of surface reverberation, *Geophysics*, *51*, 1789–1800.

Menke, W. (1989), *Geophysical Data Analysis: Discrete Inverse Theory,* Acedemic, San Diego, Calif.

Nandi, P., W. S. Holbrook, S. Pearse, P. Páramo, and R. W. Schmitt (2004), Seismic reflection imaging of water mass boundaries in the Norwegian Sea, *Geophys. Res. Lett.*, *31*, L23311, doi:10.1029/2004GL021325.

Nandi, P., et al. (2006), Seismic imaging of a thermohaline staircase in the western tropical Atlantic, *Eos Trans. AGU*, *87*(36), Ocean Sci. Meet. Suppl., Abstract OS16I-01.

Noguchi, T., et al. (2006), Thermohaline interleaving in the Kuroshio Extension Front: Seismic reflection imagery and in situ measurements, *Eos Trans. AGU*, *87*(36), Ocean Sci. Meet. Suppl., Abstract OS16I-06.

Páramo, P., and W. S. Holbrook (2005), Temperature contrasts in the water column inferred from amplitude-versus-offset analysis of acoustic reflections, *Geophys. Res. Lett.*, *32*, L24611, doi:10.1029/2005GL024533.

Pinheiro, L. M., et al. (2006), Detailed 2-D imaging of the Mediterranean Outflow and Meddies off W Iberia from multichannel seismic data, *Eos Trans. AGU*, *87*(36), Ocean Sci. Meet. Suppl., Abstract OS13I-02.

Roy, L., M. K. Sen, D. Blankenship, P. L. Stoffa, and T. Richter (2005), Inversion and uncertainty estimation of gravity data using simulated annealing: An application over Lake Vostok, East Antarctica, *Geophysics*, *70*, J1–J12.

Sen, M. K., and I. G. Roy (2003), Computation of differential seismograms and iteration adaptive regularization in prestack waveform inversion, *Geophysics*, *68*, 2026–2039.

Seymour, J. C., et al. (2006), Velocity structure of a Loop Current eddy using the gradient-current method on a seismic section from the Gulf of Mexico, *Eos Trans. AGU*, *87*(36), Ocean Sci. Meet. Suppl., Abstract OS13I-05.

Singh, S. C., T. A. Minshull, and G. D. Spence (1993), Velocity structure of a gas hydrate reflector, *Science*, *260*, 204–207.

Tarantola, A. (1987), *Inverse Problem Theory: Methods for Data Fitting and Model Parameter Estimation*, Elsevier, New York.

Tsuji, T., T. Noguchi, H. Niino, T. Matsuoka, Y. Nakamura, H. Tokuyama, S. Kuramoto, and N. Bangs (2005), Two-dimensional mapping of fine structures in the Kuroshio Current using seismic reflection data, *Geophys. Res. Lett.*, *32*, L14609, doi:10.1029/2005GL023095.

Warner, M. (1990), Absolute reflection coefficients from deep seismic reflections, *Techtonophysics*, *173*, 15–23.

White, N., et al. (2006), Seismic imaging of fronts associated with Antarctic Circumpolar Current near Drake Passage, *Eos Trans. AGU*, *87*(36), Ocean Sci. Meet. Suppl., Abstract OS16I-04.

Wood, W. T. (1999), Simultaneous deconvolution and wavelet inversion as a global optimization, *Geophysics*, *64*, 1108–1115.

Wood, W. T., P. L. Stoffa, and T. H. Shipley (1994), Quantitative detection of methane hydrate through high-resolution seismic velocity analysis, *J. Geophys. Res.*, *99*, 9681–9695.

W. S. Holbrook, Department of Geology and Geophysics, University of Wyoming, 1000 East University Avenue, Dept. 3006, Laramie, WY 82071-3006, USA.

M. K. Sen and P. L. Stoffa, Institute for Geophysics, University of Texas at Austin, Austin, TX, USA.

W. T. Wood, Code 7432, Naval Research Laboratory, Stennis Space Center, MS 39529, USA. (warren.wood@nrlssc.navy.mil)